Calibrating stellar velocity dispersions based on spatially resolved h-band spectra for improving the mbh–σ∗ relation

Kang, Wol-Rang; Woo, Jong-Hak; Schulze, Andreas; Riechers, Dominik A.; Kim, Sang Chul; Daeseong, Park; Smolčić, Vernesa

The Astrophysical Journal, 767:26 (11pp), 2013 April 10 doi:10.1088/0004-637X/767/1/26

CALIBRATING STELLAR VELOCITY DISPERSIONS BASED ON SPATIALLY RESOLVED *H*-BAND SPECTRA FOR IMPROVING THE $M_{\rm BH}$–σ_* RELATION

Wol-Rang Kang[1], Jong-Hak Woo[1,7], Andreas Schulze[2], Dominik A. Riechers[3,4], Sang Chul Kim[5], Daeseong Park[1], and Vernesa Smolcic[6]
[1] Astronomy Program, Department of Physics and Astronomy, Seoul National University, 1 Gwanak-ro Gwanak-gu, Seoul, 151-742, Republic of Korea; woo@astro.snu.ac.kr
[2] Kavli Institute for Astronomy and Astrophysics, Peking University, 100871 Beijing, China
[3] Astronomy Department, Cornell University, 220 Space Science Building, Ithaca, NY 14853, USA
[4] Astronomy Department, California Institute of Technology, MC 249-17, 1200 East California Boulevard, Pasadena, CA 91125, USA
[5] Korea Astronomy and Space Science Institute, Daejeon 305-348, Republic of Korea
[6] Physics Department, University of Zagreb, Bijenička cesta 32, 10002 Zagreb, Croatia
Received 2013 January 20; accepted 2013 February 19; published 2013 March 21

ABSTRACT

To calibrate stellar velocity dispersion measurements from optical and near-IR stellar lines, and to improve the black hole mass ($M_{\rm BH}$)–stellar velocity dispersion (σ_*) relation, we measure σ_* based on high-quality *H*-band spectra for a sample of 31 nearby galaxies, for which dynamical $M_{\rm BH}$ is available in the literature. By comparing velocity dispersions measured from stellar lines in the *H*-band with those measured from optical stellar lines, we find no significant difference, suggesting that optical and near-IR stellar lines represent the same kinematics and that dust effect is negligible for early-type galaxies. Based on the spatially resolved rotation and velocity dispersion measurements along the major axis of each galaxy, we find that a rotating stellar disk is present for 80% of galaxies in the sample. For galaxies with a rotation component, σ_* measured from a single aperture spectrum can vary by up to ∼20%, depending on the size of the adopted extraction aperture. To correct for the rotational broadening, we derive luminosity-weighted σ_* within the effective radius of each galaxy, providing uniformly measured velocity dispersions to improve the $M_{\rm BH}$–σ_* relation.

Key words: galaxies: bulges – galaxies: kinematics and dynamics – infrared: galaxies – techniques: spectroscopic

Online-only material: color figures

1. INTRODUCTION

The black hole mass ($M_{\rm BH}$) correlation with host galaxy properties has been one of the main issues in understanding galaxy evolution and black hole growth. In particular, the relatively tight correlation between $M_{\rm BH}$ and stellar velocity dispersion ($M_{\rm BH}$–σ_*) has been reported for nearby galaxies with dynamically measured $M_{\rm BH}$ (Ferrarese & Merritt 2000; Gebhardt et al. 2000a), as well as present-day active galaxies with $M_{\rm BH}$ determined from reverberation-mapping results (Onken et al. 2004; Woo et al. 2010). While early studies claimed a remarkably tight $M_{\rm BH}$–σ_* relation with its intrinsic scatter below ∼0.3 dex (e.g., Tremaine et al. 2002), recent studies showed a larger intrinsic scatter and a steeper slope due to the increased sample size, inclusion of more diverse galaxies, i.e., late-type and pseudobulge galaxies, and the improvements of $M_{\rm BH}$ measurements based on better dynamical modeling and data (Ferrarese & Ford 2005; Graham 2008; Gültekin et al. 2009a; McConnell et al. 2011, 2012).

In understanding BH–galaxy coevolution, the present-day $M_{\rm BH}$–σ_* relation sets a local calibration point as most observational studies investigated cosmic evolution of the $M_{\rm BH}$–σ_* relation by measuring an offset from the local relationship (e.g., Woo et al. 2006, 2008; Bennert et al. 2010, 2011b). At the same time, the present-day $M_{\rm BH}$–σ_* relation has been used for calibrating the $M_{\rm BH}$ of active galactic nuclei (AGNs), which is determined from the kinematics of sub-pc scale broad-emission line region. The unknown viral factor for converting the line-of-sight velocity of broad-line region gas to the intrinsic velocity has been empirically determined by matching the $M_{\rm BH}$–σ_* relation of quiescent and active galaxies at z ∼ 0 (Onken et al. 2004; Woo et al. 2010; Park et al. 2012). Thus, defining the $M_{\rm BH}$–σ_* relation in the local universe is of importance to unveil the nature of BH–galaxy coevolution.

Stellar kinematics studies based on the near-IR stellar lines became powerful as near-IR spectrographs combined with laser-guide star adaptive optics provides the best spatial resolution for the ground-based facilities (e.g., Watson et al. 2008). Moreover, measuring σ_* in the near-IR is more promising for AGN host galaxies since AGN-to-star flux ratios are much more favorable in the near-IR (Dasyra et al. 2007; Watson et al. 2008; Woo et al. 2010) while it is almost impossible to measure σ_* in the optical for host galaxies of high-luminosity QSOs.

Despite the increasing usage of near-IR spectra for probing stellar kinematics, a proper comparison between optical and near-IR measurements is still lacking. By measuring velocity dispersion of 25 early-type galaxies based on the CO absorption band head at 2.29 μm in the *K*-band, Silge & Gebhardt (2003) claimed that velocity dispersion measured from near-IR stellar lines was systematically smaller by 10–30% than that measured from optical stellar lines. In contrast, Rothberg & Fischer (2010) reported that optical and near-IR velocity dispersions were consistent for a sample of 23 early-type galaxies, by comparing σ_* measured from the CO band heads in the *K*-band, with σ_* measured from the Ca II triplet. Vanderbeke et al. (2011) also measured velocity dispersion based on the CO band heads for a sample of 22 early-type galaxies, and presented consistent results with respect to optical σ_*. The discrepancy among various studies may have resulted from the systematic uncertainties of the velocity dispersion measurements since the

[7] Author to whom any correspondence should be addressed.

line dispersion was measured from intrinsically broad CO band heads in the *K*-band and template mismatch could be very strong (see Silge & Gebhardt 2003). In contrast, the *H*-band spectral range (∼1.6–1.7 μm) contains many more stellar lines, e.g., Si I, CO, and Mg I than the *K*-band, and is possibly less susceptible to template mismatch although the presence of strong sky OH lines is a downside. To utilize the *H*-band stellar lines for studying stellar kinematics, a proper comparison is required between σ_* measured from *H*-band spectra with that measured from optical spectra stellar lines.

To derive reliable σ_* to represent the kinematics of the pressure-supported bulge or spheroidal component, the effect of the rotation component should be corrected for. In the case of galaxies with a rotating stellar disk, the line-of-sight velocity dispersion can be easily overestimated due to rotational broadening if a large aperture is used to extract a spectrum (e.g., Bennert et al. 2011a; Harris et al. 2012). The effect of rotational broadening is stronger for more edge-on stellar disks, potentially producing systematic bias. Thus, it is important to correct for rotational broadening.

In this paper, we measure the stellar velocity dispersion of 31 nearby galaxies using high-quality *H*-band spectra. We compare σ_* measurements based on stellar lines in the *H*-band with optical σ_* measurements from the literature. We also correct for the rotation and aperture effect based on the spatially resolved kinematics measurements to improve the $M_{\rm BH}$–σ_* relation. The paper is organized as follows. We describe sample selection, observations, and data reduction in Section 2. In Section 3, we present σ_* measurements, and the effects of rotation and aperture size. In Section 4, we compare our *H*-band σ_* measurements with optical σ_* from the literature, and derive the $M_{\rm BH}$–σ_* relation for early-type galaxies based on the rotation-corrected σ_*. The main results are summarized in Section 5.

2. OBSERVATIONS AND DATA REDUCTION

2.1. Sample Selection and Observations

To directly compare optical and near-IR stellar velocity dispersions and to calibrate the $M_{\rm BH}$–σ_* relation, we select 31 nearby galaxies from the $M_{\rm BH}$–σ_* sample (e.g., Gültekin et al. 2009a), for which dynamical $M_{\rm BH}$ measurements and optical σ_* measurements are available. The sample is mainly composed of early-type galaxies (20 ellipticals, 8 lenticulars, and 3 spirals) and spans a wide range in σ_* from 67 km s^{-1} to 385 km s^{-1} as listed in Table 1. Also, it covers three orders of magnitude in $M_{\rm BH}$ and constitutes about half the sample size of galaxies with dynamical $M_{\rm BH}$ measurements (McConnell & Ma 2013).

Observations were performed at the Palomar Hale 5 m telescope using the near-IR spectrograph TripleSpec, simultaneously covering the wavelength range from 1.0 μm to 2.4 μm. In this work we only employ the *H*-band spectra centered at ∼1.7 μm, as it covers many stellar absorption lines suitable for the σ_* measurement. We place an $1'' \times 30''$ long-slit along the major axis of each galaxy. The spectral resolution of TripleSpec is $R = 2500$–2700, corresponding to a Gaussian dispersion ∼50 km s^{-1}. As the lowest optical σ_* is 67 km s^{-1} (for NGC 7457), this spectral resolution is suitable for our study.

For sky subtraction, in particular for the strong OH sky emission lines, we also observed blank sky, offset by several arc minutes from each galaxy, since the size of each galaxy is larger than the slit length and fills the entire slit. We divide the total exposure time into segments of 200 second exposures to avoid saturation in the *K*-band. The total on-source exposure time ranges from 600 to 1000 s depending on the magnitude of individual galaxies (see Table 1). We observed several A0V stars each night to correct for telluric lines. We also observed 11 K- and M-type giant stars as velocity templates for the stellar velocity dispersion determination.

2.2. Data Reduction

We performed standard data reduction, i.e., bias subtraction, flat-fielding and wavelength calibration using a series of IRAF scripts, then extracted one-dimensional spectra using various extraction windows. For telluric absorption correction, we constructed a telluric line template for each observing night, based on the spectra of A0V stars observed during the night. For each A0V star, we fitted their Brackett lines with double Gaussians and normalized the spectra by its continuum. Dividing the observed A0V star spectrum by this model spectrum provides a telluric template. We combined all telluric templates to construct a mean template for a given night. Then, we used the template to correct the galaxy spectra for telluric absorption lines.

To investigate the effect of galaxy rotation on stellar velocity dispersion measurements, we extracted spatially resolved spectra from a number of small extraction windows (4–16 pixels) along the galaxy's major axis, which were allowed to overlap with each other and to slightly increase at larger radii for obtaining better signal-to-noise ratio (S/N). The resolution for spatial binning depends on the distance to each galaxy. Typically ∼10 spectra were extracted within a fraction of the $R_{\rm e}$ (see Section 3.5 for details).

A series of single-aperture spectra were also extracted using various aperture sizes in order to investigate the aperture effect. Many previous studies used spatially unresolved σ_* measurements, which were affected by line broadening due to galaxy rotation. This leads to an overestimation of the galaxy's σ_*, depending on how much rotation is included in the extraction aperture. Thus, the choice of different aperture sizes can affect the σ_* measurement as presented in Section 3.4. In contrast, we can correct the σ_* measurement for the rotational broadening using our spatially resolved spectra. Details on this correction are presented in Sections 3.4 and 3.5.

3. ANALYSIS

3.1. Stellar Velocity Dispersion Measurements

We measured the stellar velocity dispersion of 31 galaxies in the sample using the stellar lines in the 1.57–1.72 μm range, i.e., CO(4–1) 1.58 μm, Si I 1.59 μm, CO(5–2) 1.6 μm, CO(6–3) 1.62 μm, CO(7–4) 1.64 μm, CO(8–5) 1.66 μm, and Mg I 1.71 μm (see Figure 1). Using the Gauss–Hermite Pixel Fitting software (van der Marel 1994; Woo et al. 2004, 2005, 2006), we performed χ^2 minimization in fitting the galaxy spectra directly in pixel space to stellar template spectra broadened by a Gaussian kernel with velocity widths ranging from 50 to 350 km s^{-1}. The continua of the spectra of the template stars are fitted with low-order (2–3) polynomials while the Fe II emission line at 1.65 μm, bad pixels and residuals from sky line subtraction were masked out before the fitting.

3.2. Template Mismatch

Since the σ_* measurement is affected by the choice of template star, it is necessary to quantify the uncertainty due to the template mismatch. Using 11 velocity template stars of various spectral types, namely, K0 III, K1 III, K2 III, K5III,

Table 1
Sample Selection and Observing Log

Galaxy	R.A. (J2000)	Decl. (J2000)	Type	Dist.	Spatial Scale	R_e	Ref.	M_{BH}	Ref.	UT Date	T_{EXP}	S/N	PA
				(Mpc)	(kpc/1″)	(kpc)		($10^8\ M_\odot$)			(s)		(°)
(1)	(2)	(3)	(4)	(5)	(6)	(7)	(8)	(9)	(10)	(11)	(12)	(13)	(14)
N221	00 42 41.87	+40 51 57.2	E2	0.86	0.0037	0.24	1	0.026 ± 0.005	25, 6	2010 Jan 1	600	414	170
N821	02 08 21.04	+10 59 41.1	E4	25.5	0.1202	15.7	2	1.7 ± 0.7	25, 7	2010 Jan 1	600	133	25
N1023	02 40 23.90	+39 03 46.3	SB0	12.1	0.0442	1.1	2	0.4 ± 0.04	25, 8	2010 Jan 1	600	320	87
N1068	02 42 40.83	−00 00 48.4	Sb	15.4	0.0788	2.9	2	0.086 ± 0.003	5, 9	2010 Jan 1	600	455	13
N2778	09 12 24.35	+35 01 39.4	E2	24.2	0.1420	3.0	1	$0.16^{0.09}_{-0.102}$	4	2009 May 22	600	158	40
N2787	09 19 18.90	+69 12 11.9	SB0	7.9	0.0482	0.27	2	$0.41^{0.04}_{-0.05}$	25, 10	2009 May 25	600	247	109
N3031	09 55 33.17	+69 03 55.1	Sb	4.1	0.0179	3.0	2	$0.8^{0.2}_{-0.11}$	25, 11	2010 Jan 1	600	393	149
N3115	10 05 13.80	−07 43 08.0	S0	10.2	0.0460	2.9	2	$8.9^{+5.1}_{-2.7}$	25, 12	2010 Jan 1	600	362	40
N3245	10 27 18.52	+28 30 24.8	S0	22.1	0.0911	1.0	2	$2.1^{+0.5}_{-0.6}$	25, 13	2009 May 22	600	247	177
N3377	10 47 42.36	+13 59 08.8	E6	11.7	0.0461	3.9	2	1.8 ± 0.9	25, 7	2010 Jan 1	600	244	41
N3379	10 47 49.75	+12 34 54.6	E0	11.7	0.0631	2.7	2	$4.2^{+1.0}_{-1.1}$	25, 14	2009 May 22	600	307	73
N3384	10 48 16.90	+12 37 42.9	SB0	11.7	0.0488	0.48	2	0.11 ± 0.05	25, 7	2010 Jan 1	600	254	53
N3607	16 12 54.64	+18 03 06.3	E1	19.9	0.0665	4.3	3	$1.4^{+0.4}_{-0.5}$	25, 12	2010 Jan 1	800	229	125
N3608	11 16 59.07	+18 08 54.6	E1	23.0	0.0869	3.9	2	4.7 ± 1.0	25, 7	2009 May 25	800	252	75
N4258	12 18 57.54	+47 18 14.3	SABbc	7.2	0.0310	0.66	2	0.367 ± 0.001	25, 16	2009 Mar 5	600	229	150
N4261	12 19 23.21	+05 49 29.7	E2	33.4	0.1551	5.8	2	5.3 ± 1.1	25, 17	2009 May 25	600	203	160
N4291	12 20 17.60	+75 22 15.0	E2	25.0	0.1218	2.0	2	9.8 ± 3.1	25, 7	2010 Jan 1	800	164	110
N4342	12 23 39.12	+07 03 12.9	S0	18.0	0.0520	0.21	2	$4.6^{+2.6}_{-1.5}$	25, 18	2009 Mar 5	800	104	168
N4374	12 25 03.74	+12 53 13.1	E1	17.0	0.0735	7.8	2	$9.2^{+1.0}_{-0.8}$	25, 19	2010 Jan 1	600	250	122.5
N4459	12 29 00.13	+13 58 42.5	E2	17.0	0.0839	13.7	2	$0.7^{+0.13}_{-0.14}$	25, 10	2009 Mar 5	600	206	110
N4473	12 29 48.95	+13 25 46.1	E4	17.0	0.1555	2.1	2	$0.89^{+0.45}_{-0.44}$	25, 7	2009 Mar 5	600	170	100
N4486	12 30 49.42	+12 23 28.0	E1	17.0	0.0906	6.0	2	$62.0^{+3.0}_{-4.0}$	25, 20	2009 May 22	600	168	153
N4564	12 36 27.01	+11 26 18.8	S0	17.0	0.0791	3.0	1	0.88 ± 0.24	25, 7	2009 May 25	600	272	47
N4596	12 39 56.16	+10 10 32.4	SB0	18.0	0.1296	1.5	2	$0.84^{+0.36}_{-0.25}$	25, 10	2009 May 25	600	208	75
N4649	12 43 40.19	+11 33 08.9	E2	16.5	0.0774	7.2	2	$47.0^{+11.0}_{-10.0}$	25, 21	2009 May 22	600	221	105
N4697	12 48 35.70	−05 48 03.0	E6	12.4	0.0860	6.9	2	2.0 ± 0.2	25, 7	2010 Jan 1	600	260	70
N4742	12 51 47.92	−10 27 17.1	E4	16.4	0.0880	1.6	2	0.14 ± 0.05	24	2009 May 25	600	355	75
N5845	15 06 00.90	+01 38 01.4	E3	28.7	0.1005	0.42	2	$4.9^{+1.5}_{-1.6}$	25, 7	2009 May 22	600	274	141
N6251	16 32 31.97	+82 32 16.4	E1	106.0	0.5134	10.0	2	6.0 ± 2.0	25, 22	2009 May 22	600	141	21
N7052	21 18 33.13	+26 26 48.7	E3	70.9	0.3238	9.1	2	$4.0^{+2.8}_{-1.6}$	25, 23	2009 May 25	1000	185	62
N7457	23 01 00.05	+30 08 43.4	S0	14.0	0.0563	4.8	1	0.10 ± 0.06	5, 7	2009 May 25	600	131	125

Notes. Column 1: NGC galaxy catalogue name. Column 2: right ascension. Column 3: declination. Column 4: morphological types. Column 5: distance. Column 6: spatial scale. Columns 7–8: effective radius and reference. Columns 9–10: black hole mass and their reference. Column 11: observation date. Column 12: total exposure time. Column 13: average signal-to-noise ratio within ±5 pixel aperture. Column 14: position angle.

References. (1) Marconi & Hunt 2003; (2) Graham 2008; (3) Sani et al. 2011; (4) Gültekin et al. 2009a; (5) McConnell et al. 2011; (6) Verolme et al. 2002 (7) Schulze & Gebhardt 2011; (8) Bower et al. 2001; (9) Lodato & Bertin 2003; (10) Sarzi et al. 2001; (11) Devereux et al. 2003; (12) Emsellem et al. 1999; (13) Barth et al. 2001; (14) van den Bosch & de Zeeuw 2010; (15) Gültekin et al. 2009b; (16) Herrnstein et al. 2005; (17) Ferrarese et al. 1996; (18) Cretton & van den Bosch 1999; (19) Walsh et al. 2010; (20) Gebhardt et al. 2011; (21) Shen & Gebhardt 2010; (22) Ferrarese & Ford 1999; (23) van der Marel & van den Bosch 1998; (24) Tremaine et al. 2002; (25) McConnell & Ma 2013.

two M0 III, M1 III, two M2 III, M3 III, and M5 III, which were observed with the same instrumental setup during our observing runs, we measured and compared σ_* for individual galaxies in the sample, in order to investigate the variation in the σ_* measurement caused by template mismatch. Then, we accounted for template mismatch in the determination of σ_* by averaging σ_* measurements using various template stars.

To compare the overall spectral shapes, we present the spectra of the individual template stars, after broadening them with a Gaussian velocity (red thick lines) in Figure 1. The observed spectrum of NGC 1023 is overplotted (black lines) to demonstrate the template mismatch. In the stellar spectra, the line strength of the CO absorption lines increases toward later-type stars (from upper panels to lower panels). This trend is in particular clearly shown for the CO(6–3) line at 1.62 μm and also for the Mg I line at 1.71 μm. On the other hand, the Si I line strength shows no strong variation with spectral type. The comparison in Figure 2 clearly shows that spectra of K-type stars provide a poor match to the observed galaxy spectrum in this wavelength range, while spectra of M-type stars can fit the observed galaxy spectrum reasonably well.

In Figure 2, we compare the multiple measurements of σ_* of NGC 1023, using each template star for the fitting. As expected from Figure 1, the σ_* measured from M-type stars shows small variation, while σ_* measured from K-type stars exhibits a larger scatter, suggesting that M-type stars provide a fair representation

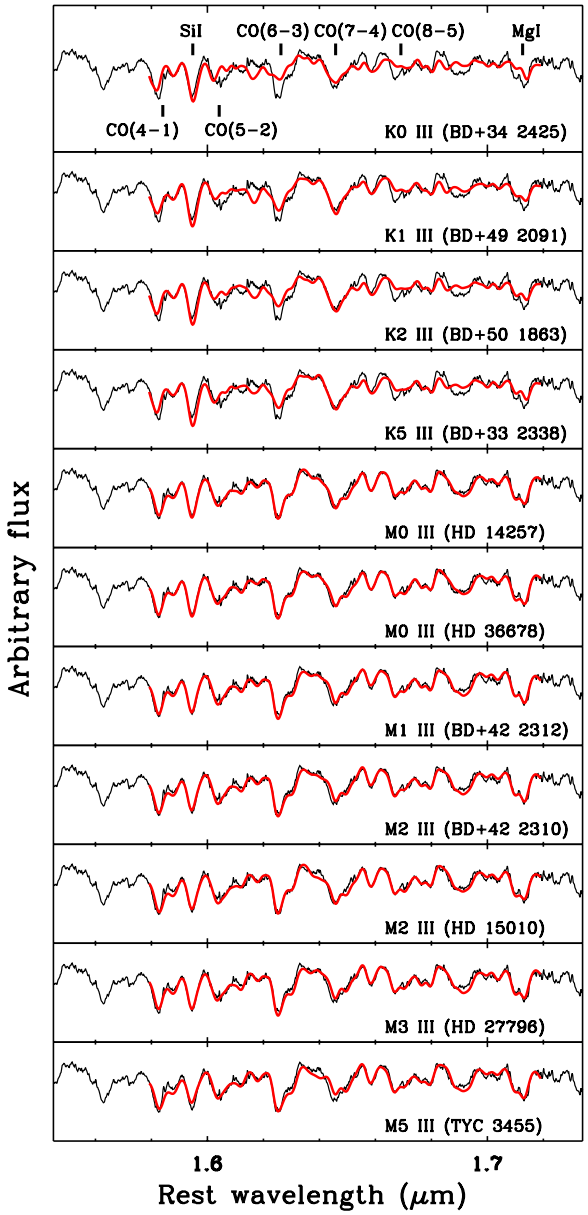

Figure 1. Normalized spectra of template stars. The template star spectra (thick red solid line) are compared with the spectra of NGC 1023 (thin black solid line). The template star is broadened with a Gaussian velocity kernel. Individual template stars show different line strengths, particularly for the CO absorption line. The K-type star templates provide a poor fit to the galaxy spectrum. In the top panel, we marked several individual stellar lines with black tick masks (from left, CO(4–1), Si I, CO(5–2), CO(6–3), CO(7–4), CO(8–5), and Mg I).

(A color version of this figure is available in the online journal.)

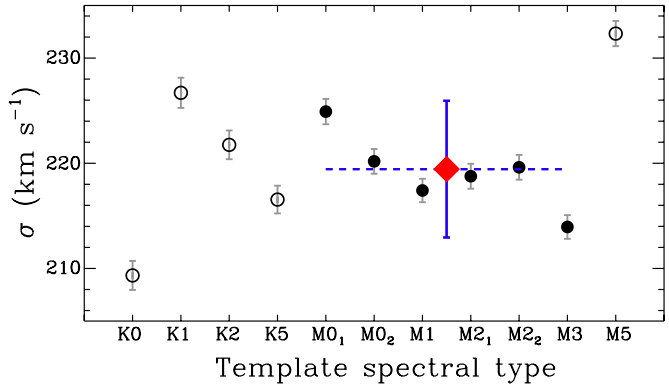

Figure 2. Comparison of the measured stellar velocity dispersion of NGC 1023 using different template stars. Filled circles denote M0 III, M1 III, M2 III, and M3 III type stars, which were used for calculating the mean stellar velocity dispersion. Open circles denote M5 III and K-type template stars. The mean σ_* is given by the red diamond and the standard deviation of the measurements is included in the uncertainty denoted by the blue solid error bar. The blue dashed line indicates the range of template stars used for calculating the mean stellar velocity dispersion.

(A color version of this figure is available in the online journal.)

of the luminosity-weighted stellar population in the *H*-band. Therefore, we excluded the measurements from K-type stars and calculated the mean σ_* based on the six M-type stars. Since the M5 III star shows slightly different line shapes compared to other M-type stars (see Figure 1), we also excluded the measurement based on the M5 III template. After calculating the standard deviation of the measurements from six M-type stars as the uncertainty of template mismatch, we added the uncertainty of template mismatch to the mean measurement errors from six M-type stars in quadrature, in order to determine the uncertainty of σ_*. For example, the red diamond in Figure 2 indicates the mean σ_*, derived from six template stars and its uncertainty. In Figure 3, we present the normalized observed spectrum (black solid line) of each galaxy in the sample, overplotted with the best-fit model (red solid line).

3.3. Spatially Resolved Stellar Velocity Dispersions

By extracting spectra over several bins along the major axis, we obtained spatially resolved kinematics. In Figures 4 and 5 we show the radial profiles of line-of-sight velocities (upper panel) and velocity dispersions (lower panel) for each galaxy. We used the line-of-sight velocity of the galaxy center as a reference and normalized all velocities with respect to the central value. For most galaxies we extracted 9–13 spectra along the slit (in the direction of the major axis) out to $\pm 7''$ from the center. This is smaller than the slit size ($\pm 15''$) since we were not able to use outer pixels due to much lower S/N than the central bins to measure σ_* and the ABBA dither pattern along the slit.

Among the sample galaxies, we find a clear rotation component for 25 out of 31 objects. The amplitude of the projected rotation velocity ranges from $\sim$40 km s^{-1} to over 200 km s^{-1} while six galaxies, namely NGC 1068, NGC 3608, NGC 4261, NGC 4374, NGC 4486, and NGC 6251 show a weak or no rotation component. For the galaxies with a significant rotation component, we expect line broadening due to the rotation, leading to overestimation of σ_*, if a large single aperture is used for extraction. While the magnitude of this effect depends on the details of radial profiles of rotation and velocity dispersion of each galaxy, it will lead to a systematic bias if not taken into account. We will account for the rotation component in the stellar velocity dispersion measurement in the next subsection.

In the lower panels of Figures 4 and 5, we show the stellar velocity dispersion profiles along the major axis. While stellar velocity dispersion decreases from the center to the outer regions for most galaxies, several galaxies, e.g., NGC 1068, NGC 4261, NGC 4374, NGC 4596, and NGC 7052, do not show such a decreasing trend of σ_*, but rather show irregular shapes; flat, increasing or asymmetric trends as similarly reported by previous studies based on optical kinematics studies (e.g., Dressler 1984; Bender et al. 1994; Kent 1990; Pinkney et al. 2003).

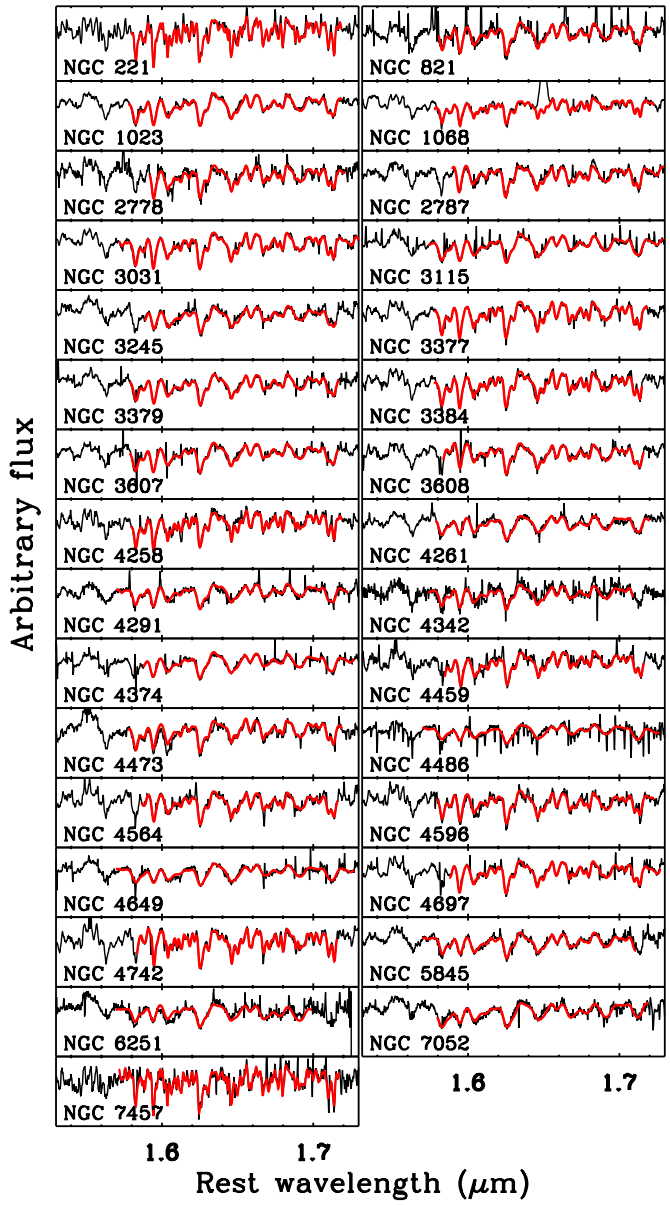

Figure 3. Normalized spectra of the 31 galaxies and their best-fit models. The broadened template star spectra (thick red solid line) fit the observed galaxy spectra (thin black solid line) reasonably well. Residuals of OH sky emission lines (sharp features in Figure 1) and the AGN Fe II emission line (e.g., in NGC 1068) were masked out before fitting.

(A color version of this figure is available in the online journal.)

3.4. Aperture Size Effect

We investigate the effect of using different aperture sizes on the measured stellar velocity dispersion by directly measuring σ_* from apertures of increasing size. In Figure 6 we present the σ_* measurements as a function of aperture size, after normalizing them to the σ_* measured from the smallest aperture (4–10″). We find three different trends (increasing, flat and decreasing) of σ_* with increasing aperture size. The 8 galaxies shown in the upper panels exhibit an increase of σ_* as a larger aperture size is used, while for 13 galaxies shown in the lower panels, σ_* decreases with increasing aperture size. These galaxies show variation of σ_* up to 20% as aperture size changes. In contrast, 10 galaxies (middle panels) do not show clear change of σ_* as a function of aperture size.

Thus, when measuring σ_* from a large aperture it is possible to either overestimate or underestimate σ_*. The magnitude and direction of this bias depends on two factors: (1) the overestimation caused by rotational line broadening and (2) the natural decrease of σ_* as a function of radius. The galaxies in the upper panels in Figure 6 are dominated by the first effect. They show relatively strong galaxy rotation and only a mild decrease in their velocity dispersion profile, as shown in Figures 4 and 5, leading to a net increase in σ_* with increasing aperture size. For these galaxies, when the extraction aperture covers outer parts of the galaxy where the rotation curves flatten, the aperture effect on σ_* also flattens. This is clearly seen, for example, in the case of NGC 3384, which shows a flattening of σ_* beyond the third bin, corresponding to the flattening of the rotation curve in Figure 4. NGC 4742 even shows a decrease in σ_* beyond the radius where the rotation curves becomes flat.

The decreasing σ_* trend for the galaxies in the lower panels of Figure 6 can be explained in a similar way. For these galaxies the decrease in σ_* profile is dominating over line broadening due to rotation. For example, NGC 4486 shows the largest variation in σ_* as a function of aperture size since it has no significant rotation component while the velocity dispersion profile is strongly decreasing toward larger radii. Similarly, NGC 3608 and NGC 4649 also show strong decrease, which is dominated by the strong decrease in σ_* with radius. In contrast, there are galaxies, e.g., NGC 821, where the effect from the rotation curve and the decreasing σ_* profile are roughly of the same order, leading to a small net variation of σ_* measured from different apertures.

3.5. Correction of the Galaxy Rotation Effect

As discussed above, σ_* measured within a certain aperture will be susceptible to line broadening by galaxy rotation. In contrast, the spatially resolved stellar velocity dispersions, represented in Figures 4 and 5, do not suffer rotational broadening. Thus, we can use these measurements to compute a rotation-corrected σ_*. We compute luminosity-weighted σ_* within a radius R:

$$\sigma_R = \frac{\int_{-R}^{R} \sigma_*(r)\, I(r)\, dr}{\int_{-R}^{R} I(r)\, dr}, \quad (1)$$

where $I(r)$ is the surface brightness profile of the galaxy and R is the outer radius within which we compute σ_*. Using the spectral images, we measure the surface brightness profile of each galaxy by fitting with two Gaussian models, and use this fit to compute the luminosity-weight for σ_* measured at each radius. We chose an outer radius R for each galaxy based on the R_e (see Table 1). For 20 galaxies, we were able to measure spatially resolved σ_* only at the central parts, due to the limited spatial coverage and/or lower S/N at the outer part. Thus, we chose one-eighth of R_e as an outer radius in Equation (1). For the other 11 galaxies, we measured σ_* over a larger fraction of R_e (one-fourth to unity) as an outer radius and corrected for the rotation component as listed in Table 2.

In Figure 7 we illustrate the effect of the correction for galaxy rotation. Here, σ_R is the luminosity-weighted σ_* within R as computed from Equation (1) while $\sigma_R(uncor)$ is measured from a single aperture with an aperture size of R. As expected, most galaxies show a decrease in velocity dispersion when accounting for the rotation component, while for galaxies without strong rotation component, the correction is marginal. Including six galaxies that show no rotation, the average correction is 6%, while the correction for individual galaxies can be up to ∼20%.

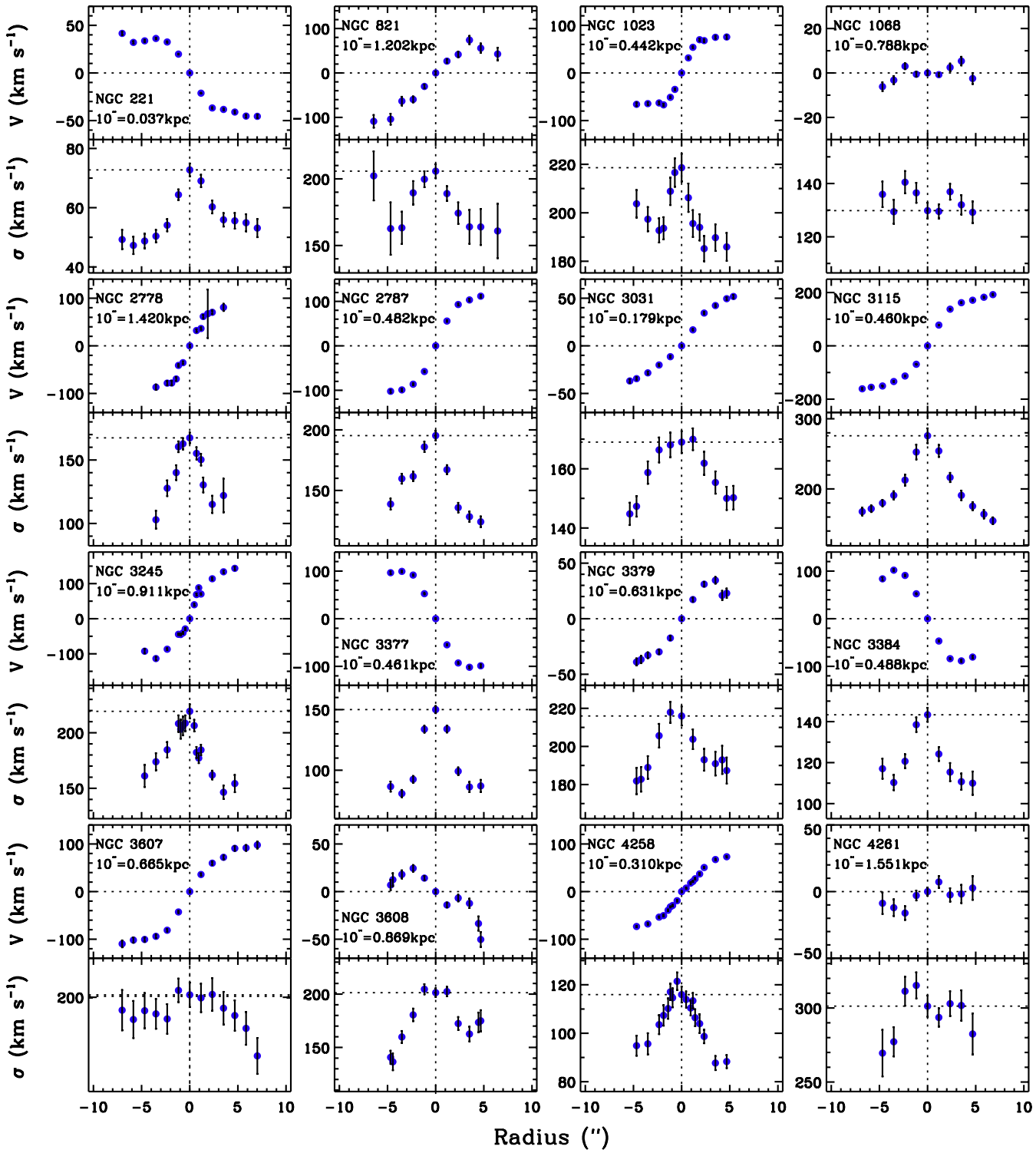

Figure 4. Line-of-sight velocities (upper panel) and stellar velocity dispersions (lower panel) along the major axis. Most galaxies show a clear rotation component and a radial decrease of σ_*. The object name and the spatial scale are shown in each upper panel.

(A color version of this figure is available in the online journal.)

The magnitude of the rotation correction tends to be smaller for more massive galaxies. NGC 7052 with the highest σ_* in the sample seems to be an outlier from this trend since it has relatively large rotation while σ_* mildly decreases within $R_e/8$. In summary, we find that stellar velocity dispersions measured from single-aperture spectra can be biased by up to ∼20%. This is consistent with the results of Bennert et al. (2011a) and Harris et al. (2012).

A possible drawback for the comparison with previous studies, that usually report σ_* measured within R_e, is the limited spatial coverage in our work, restricting our measurements to $R_e/8$. To investigate the effect on the σ_* measurement, we tested two extreme cases. First, we assumed a constant σ_* from $R_e/8$ to R_e, equal to the value at $R_e/8$. Second, we extrapolated the decreasing stellar velocity dispersion profile out to R_e. For both cases we computed the luminosity-weighted σ_* within R_e via

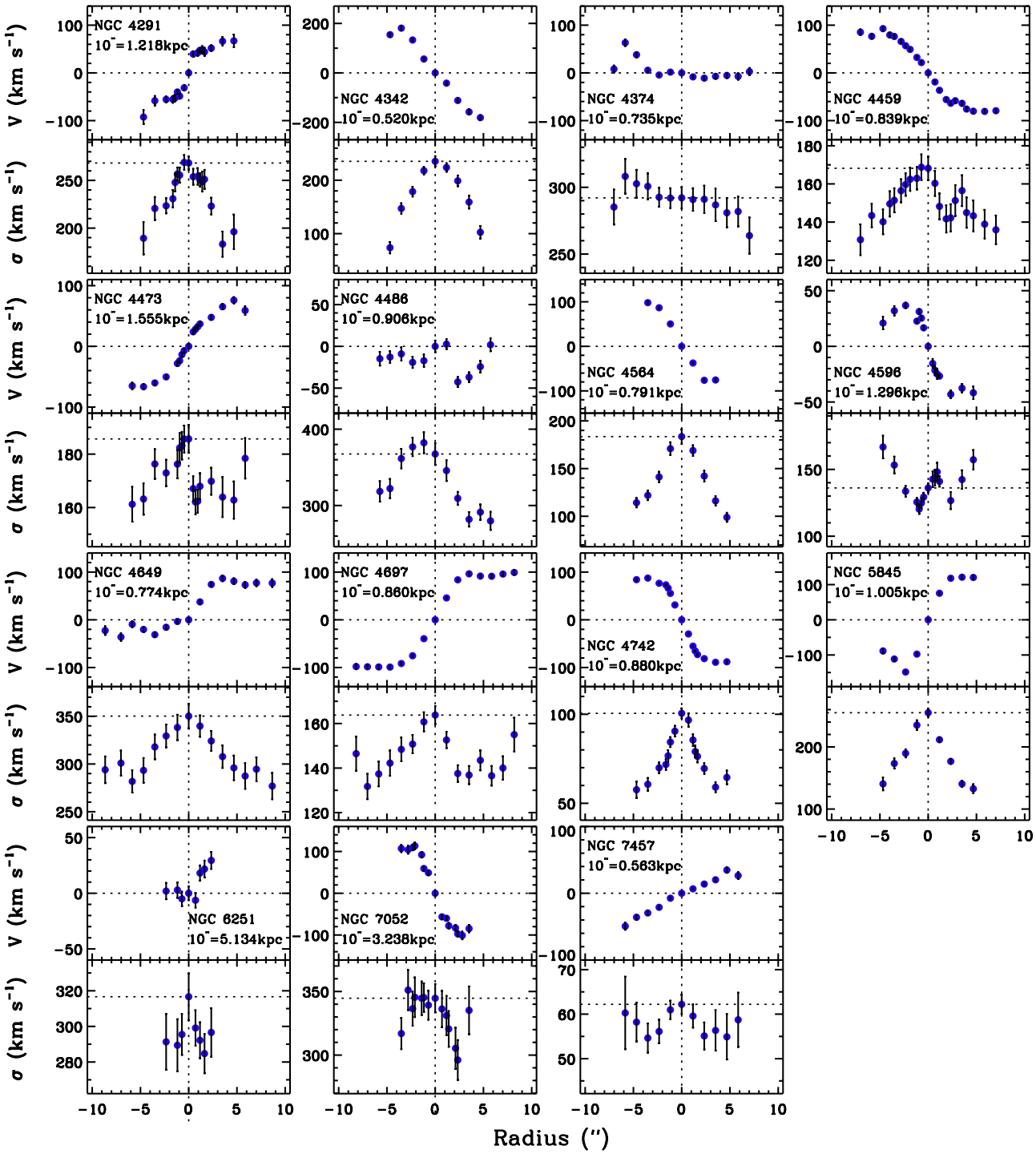

Figure 5. Same as Figure 4 for the rest of the sample.
(A color version of this figure is available in the online journal.)

Equation (1). We found that σ_* values decrease by only a few percent by increasing the outer radius from $R_e/8$ to R_e in both cases, due to the much lower luminosity weight at outer radii. Thus, our σ_* measurements within $R_e/8$ will closely resemble the value that would be measured at R_e.

4. DISCUSSION

4.1. Optical versus Near-IR Velocity Dispersions

In Figure 8 we compare the stellar velocity dispersions measured using our near-IR spectra (σ_{IR}) with the literature values measured from optical spectra (σ_{opt}). For this comparison, we collected σ_{opt} measurements from McConnell & Ma (2013), who listed their own measurements as well as previously measured values from the literature (see Table 2). Although these optical measurements were based on spatially resolved stellar kinematics and the quoted values were luminosity-weighted or averaged velocity dispersions within the R_e for most galaxies, these values were not homogeneously measured due to the various data quality and the measurement methods. In addition, some of these values in the original works were measured with a smaller aperture size than R_e or the aperture

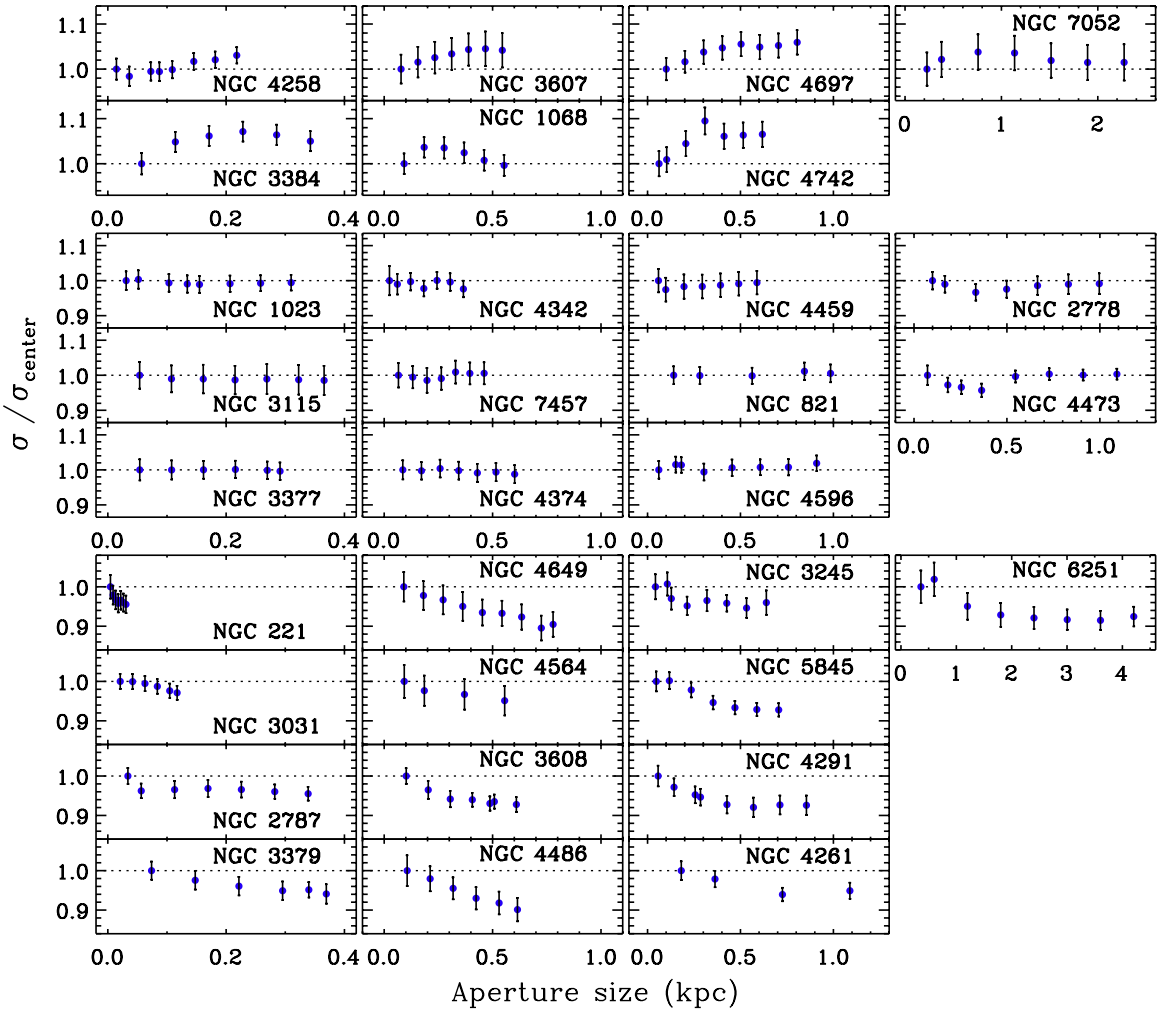

Figure 6. Stellar velocity dispersions measured from various aperture sizes. Each σ_* measurement is normalized by σ_* measured from the smallest aperture. Upper panels show the objects that have increasing trend, while lower panels show the objects with an opposite trend. Middle panels show the objects that have constant trend of σ_*. Galaxies are sorted by the distance.

(A color version of this figure is available in the online journal.)

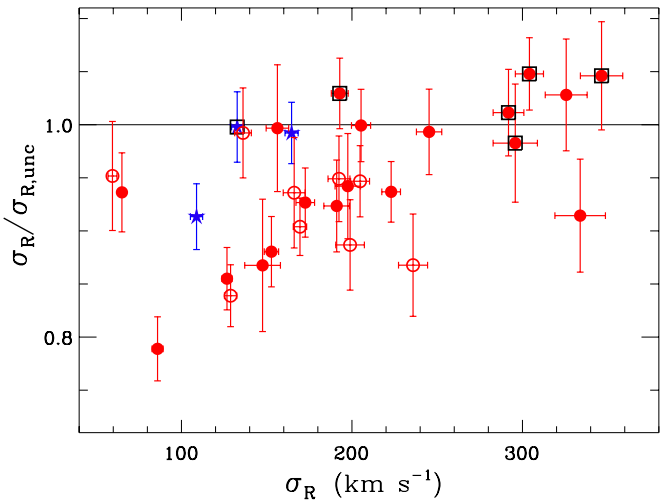

Figure 7. Ratio of velocity dispersions determined with and without rotation correction as a function of velocity dispersion. Filled and open circles represent elliptical and lenticular galaxies, respectively, while stars denote late-type galaxies. Six galaxies without a clear rotation component are marked with open squares.

(A color version of this figure is available in the online journal.)

size was not clearly stated for many cases in the original references.

Thus, we decide to compare both H-band σ_* measurements with/without rotation correction to the optical σ_* measurements. As shown in Figure 8, we find no significant difference between $\sigma_{\rm opt}$ and $\sigma_{\rm IR}$. The best fit between optical and near-IR measurements is close to a one-to-one relation with a scatter of ~0.04 dex (10%) when rotation is not corrected for $\sigma_{\rm IR}$. The lower panel in Figure 8 shows that the rotation-corrected $\sigma_{\rm IR}$ is slightly smaller than the optical σ_* at lower mass range. However, the average offset is only 7%, which is not significant compared to the measurement uncertainties of stellar velocity dispersions.

Note that McConnell & Ma (2013) included rotation in calculating luminosity-weighted σ_* by adding rotation velocity to velocity dispersion in quadrature (see their Equation (1)). Thus, the slight offset between our $\sigma_{\rm IR}$ and optical σ_* from McConnell & Ma (2013) may be explained by the rotation effect. To test this hypothesis, we derive rotation-included velocity dispersions using the same integral as adopted by McConnell & Ma (2013, Equation (1)). For these consistently measured velocity dispersions, we find that optical and IR velocity dispersions show a one-to-one relationship with a slope of 1.00 ± 0.05 and a 0.03 dex (7%) intrinsic scatter. Thus, we

Table 2
Near-IR and Optical Stellar Velocity Dispersions

Name	σ_{IR}				σ_{opt}	Ref.
	$\sigma_{R,unc}$ (km s^{-1})	σ_{R} (km s^{-1})	R (R_e)	$\sigma_{\pm 7''}$ (km s^{-1})	(km s^{-1})	
(1)	(2)	(3)	(4)	(5)	(6)	(7)
N221	70 ± 2	65 ± 2	1/8	70 ± 2	75 ± 3	1, 2
N821	207 ± 5	191 ± 8	1/8	208 ± 5	209 ± 10	3
N1023	216 ± 5	205 ± 6	1/4	217 ± 5	205 ± 10	4
N1068	133 ± 3	133 ± 3	1/8	129 ± 3	151 ± 7	5
N2778	170 ± 4	148 ± 11	1/4	161 ± 4	175 ± 8	3
N2787	188 ± 4	170 ± 4	1	186 ± 3	189 ± 9	6
N3031	166 ± 3	165 ± 4	1/8	157 ± 3	143 ± 7	7
N3115	272 ± 11	236 ± 9	1/8	272 ± 12	230 ± 11	7
N3245	203 ± 5	192 ± 6	1/2	206 ± 7	205 ± 10	7
N3377	148 ± 4	127 ± 3	1/8	147 ± 4	145 ± 7	8, 9
N3379	205 ± 4	205 ± 6	1/8	203 ± 5	206 ± 10	10, 2
N3384	154 ± 3	129 ± 4	1/2	151 ± 3	143 ± 7	3
N3607	210 ± 8	198 ± 7	1/8	210 ± 8	229 ± 11	11
N3608	187 ± 4	193 ± 5	1/8	187 ± 4	182 ± 9	3
N4258	119 ± 3	109 ± 4	1/4	111 ± 2	115 ± 10	6
N4261	290 ± 5	304 ± 8	1/8	286 ± 6	315 ± 15	12, 2
N4291	247 ± 7	245 ± 7	1/4	248 ± 7	242 ± 12	3
N4342	224 ± 5	199 ± 8	1	224 ± 5	225 ± 11	13, 2
N4374	289 ± 7	292 ± 7	1/8	290 ± 8	296 ± 14	14, 2
N4459	157 ± 7	156 ± 7	1/8	164 ± 6	167 ± 8	7
N4473	186 ± 3	173 ± 5	1/2	186 ± 3	190 ± 9	3
N4486	331 ± 11	346 ± 12	1/8	331 ± 11	375 ± 18	15
N4564	177 ± 7	166 ± 6	1/8	175 ± 7	162 ± 8	3
N4596	137 ± 3	136 ± 5	1/2	139 ± 3	136 ± 6	7
N4649	317 ± 11	326 ± 13	1/8	327 ± 11	385 ± 19	3, 15
N4697	174 ± 4	153 ± 4	1/8	172 ± 4	177 ± 8	3
N4742	109 ± 3	86 ± 3	1/4	104 ± 3	90 ± 5	7
N5845	238 ± 4	223 ± 5	1	237 ± 4	234 ± 11	9
N6251	301 ± 11	296 ± 13	1/8	290 ± 8	290 ± 14	17, 2
N7052	365 ± 14	334 ± 15	1/8	327 ± 13	266 ± 13	18
N7457	63 ± 2	60 ± 3	1/8	63 ± 2	67 ± 3	3

Notes. Column 1: object name. Column 2: *H*-band stellar velocity dispersion measured using a single aperture size *R* without rotation correction. Column 3: luminosity-weighted *H*-band σ_* within R. Column 4: aperture radius *R* used for *H*-band σ_* in units of R_e. Column 5: *H*-band velocity dispersion measured using a single aperture within $\pm 7''$. Column 6: optical stellar velocity dispersions. Column 7: reference for optical velocity dispersions.

References. (1) van der Marel et al. 1998; (2) Gebhardt et al. 2000a; (3) Pinkney et al. 2003; (4) Bower et al. 2001; (5) Nelson & Whittle 1995; (6) Gültekin et al. 2009a; (7) Kormendy & Gebhardt 2001; (8) Kormendy et al. 1998; (9) Gebhardt et al. 2003; (10) Gebhardt et al. 2000b; (11) Gültekin et al. 2009b; (12) van der Marel et al. 1990; (13) Cretton & van den Bosch 1999; (14) Bower et al. 1998; (15) Gebhardt et al. 2011; (16) McConnell et al. 2011; (17) Smith et al. 1990; (18) van den Bosch & van der Marel 1995.

conclude that σ_* measurements derived from optical and *H*-band stellar lines are consistent.

While many studies have been devoted to measure σ_* of galaxies using optical spectra, the number of σ_* studies based on near-IR data, either *H*-band or *K*-band spectra is growing. However, there are currently only few studies that actually compared the results from both wavelength regimes. For example, Silge & Gebhardt (2003) measured σ_* of a sample of 25 elliptical and lenticular galaxies using the 2.29 μm CO(2–0) band head in the *K*-band spectra. Comparing their IR results to optical velocity dispersions from the literature, they concluded that IR stellar velocity dispersions can be lower than optical stellar velocity dispersions, by up to 30%–40% and with a median offset of 11%. The inconsistency between optical and near-IR measurements is probably due to a sample bias and measurement uncertainties. First, their sample mainly consists of S0 galaxies and the systematic difference between optical and near-IR velocity dispersion in their study is mainly caused by S0 galaxies while their elliptical subsample does not show a difference between optical and near-IR measurements. Second, Silge & Gebhardt (2003) measured σ_* using solely a single CO band head in the *K*-band, which is much more susceptible to template mismatch as explained in their analysis.

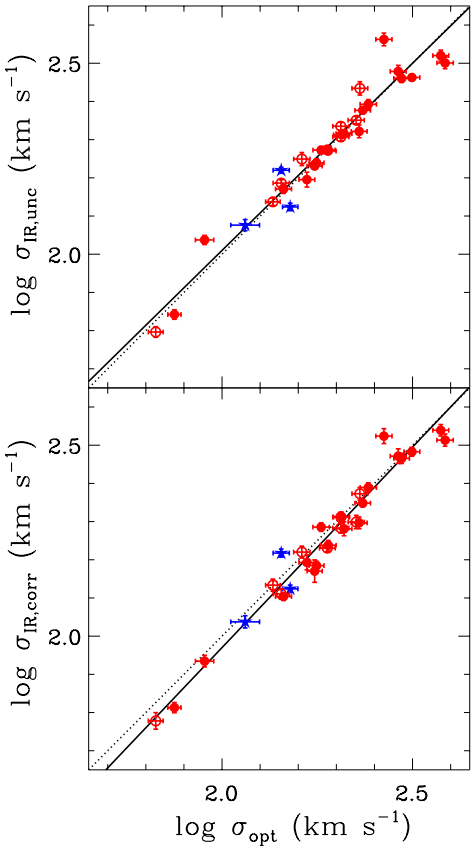

Figure 8. Comparison between *H*-band stellar velocity dispersions and optical stellar velocity dispersions from the literature. *H*-band σ_* is measured from an extraction aperture, $\pm 7''$ (top panel) or corrected for rotation effect (bottom panel). Elliptical and lenticular galaxies are denoted with filled and open circles while three late-type galaxies are indicated by filled stars. The best-fit (solid line) is consistent with a one-to-one relation (dotted line).

(A color version of this figure is available in the online journal.)

In contrast to Silge & Gebhardt (2003), Rothberg & Fischer (2010) reported no inconsistency between optical and near-IR stellar velocity dispersion measurements for elliptical galaxies. Using a sample of 23 elliptical galaxies and 14 merger remnants, they measured σ_* from stellar lines in the *K*-band spectra, i.e., CO(2–0), CO(3–1), and CO(4–2) band heads, and compare them with velocity dispersion measured from the optical Ca II triplet line, showing that optical and near-IR stellar velocity dispersions are virtually the same for elliptical galaxies. For merger remnants Rothberg & Fischer (2010) reported a discrepancy between optical and near-IR velocity dispersions, presumably due to the presence of young stellar population, which are obscured at optical wavelengths. However, for elliptical galaxies, their results indicate that optical and near-IR stellar lines represent the same kinematics and a dust effect is negligible. Similarly, a recent study by Vanderbeke et al. (2011) presented near-IR σ_* measurements also based on the CO band heads for a sample of 22 galaxies, consisting of similar numbers of ellipticals and lenticulars. Comparing with previous optical

measurements, they reported that optical and near-IR σ_* were consistent for their sample, which is consistent with our results.

In the case of velocity dispersions using *H*-band stellar lines, there has been no systematic comparison with optical velocity dispersions. Using various stellar lines in the *H*-band spectra and carefully accounting for the template mismatch problem (see Section 3.2), for the first time, we show that optical and *H*-band σ_* measurements are consistent for early-type galaxies, indicating that optical and *H*-band stellar lines represent the same kinematics and that a dust effect, i.e., obscuration at optical wavelengths, is negligible. These results are consistent with *K*-band stellar kinematics (Rothberg & Fischer 2010; Vanderbeke et al. 2011). Our results imply that near-IR σ_* measurements carried out for AGN host galaxies, for which optical measurements are more difficult to perform due to the strong AGN contribution (e.g., Woo et al. 2010), provide unbiased results, compared to optical measurements.

4.2. The M_{BH}–σ_* Relation for Early-type Galaxies

In this paper we present homogeneously measured σ_* for 31 galaxies with dynamical $M_{\rm BH}$ measurements. By accounting for galaxy rotation and implementing a uniform analysis for measuring velocity dispersions, our σ_* measurements are slightly different from previous optical values. In this section we demonstrate the effect of these new velocity dispersions on the $M_{\rm BH}$–σ_* relation by fitting the $M_{\rm BH}$–σ_* relation for 31 galaxies, for which we obtained the rotation-corrected σ_*. Results on the $M_{\rm BH}$–σ_* relation for the full sample of galaxies with dynamical $M_{\rm BH}$ will be presented in a companion paper (J.-H. Woo et al. 2013, in preparation). For this analysis, we used the most recent $M_{\rm BH}$ updates from McConnell & Ma (2013).

We fit the $M_{\rm BH}$–σ_* relation as a single-index power law:

$$\log(M_{\rm BH}/M_\odot) = \alpha + \beta \log(\sigma_*/200\,{\rm km\,s^{-1}}). \quad (2)$$

We used the FITEXY method, modified to account for intrinsic scatter in the relation (Tremaine et al. 2002; Park et al. 2012), to perform the fit as shown in Figure 9.

By fitting the $M_{\rm BH}$–σ_* relation using the optical σ_* from McConnell & Ma (2013), we obtain $\alpha = 8.27\pm0.07$, $\beta = 3.98\pm0.40$ and an intrinsic scatter of 0.38 ± 0.05 dex. Our sample has a large overlap with the sample used by Tremaine et al. (2002), and indeed we obtain consistent results for the $M_{\rm BH}$–σ_* relation. The slight difference arises mainly from a few different galaxies in both samples and from updated $M_{\rm BH}$ determinations (e.g., Schulze & Gebhardt 2011). By fitting the $M_{\rm BH}$–σ_* relation using our rotation-corrected near-IR σ_*, we find $\alpha = 8.35\pm0.08$, $\beta = 3.78\pm0.43$ and an intrinsic scatter of 0.38 ± 0.05 dex. This relation is slightly shallower than that derived from optical σ_*, but consistent within the uncertainties.

Note that the previous studies on the $M_{\rm BH}$–σ_* relation by Gültekin et al. (2009a) and McConnell & Ma (2013) explicitly included rotation in calculating luminosity-weighted σ_*. In this case, we expect systematic effect on the measured σ_* due to the random orientation of stellar disk with respect to the line of sight. To investigate this effect, we calculated σ_* by adding velocity to velocity dispersion in quadrature using Equation (1) in McConnell & Ma (2013). The result shows that rotation-included σ_* is slightly larger than rotation-corrected σ_*, particularly at low mass scale, by 0.02 dex (~5%) on average with a 0.02 (~5%) scatter. Consequently, when we replace rotation-corrected σ_* with rotation-included σ_* in fitting the $M_{\rm BH}$–σ_* relation, the slope slightly increases from 3.78 ± 0.43 to 3.97 ± 0.49 as the σ_* values increase preferentially at low mass scale, while intrinsic scatter remains the same.

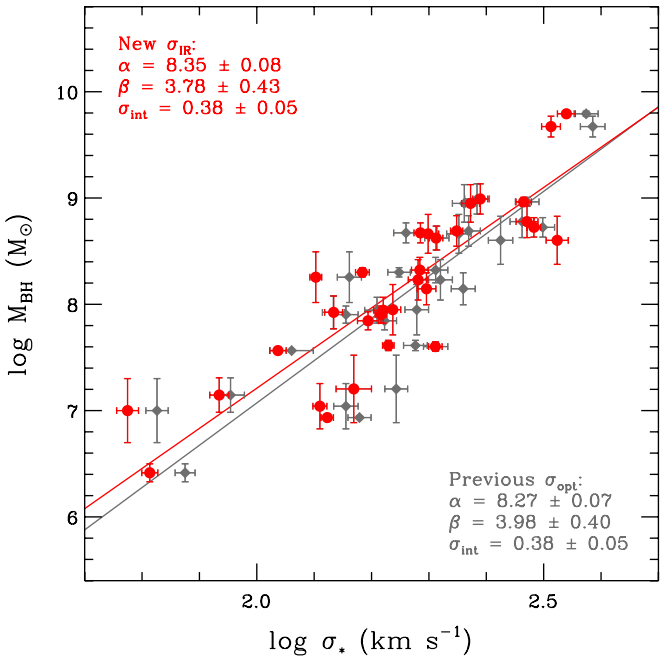

Figure 9. $M_{\rm BH}$–σ_* relation of 31 nearby galaxies, using rotation-corrected σ_* measured from our *H*-band spectra (red circles, red line) and rotation-included optical σ_* from McConnell & Ma (2013; gray diamonds, gray line), respectively. (A color version of this figure is available in the online journal.)

Although we expect that the rotation effect will systematically affect the $M_{\rm BH}$–σ_* relation (see also Graham et al. 2011), we do not clearly detect the improvement of the $M_{\rm BH}$–σ_* relation by using rotation-corrected σ_*, presumably due to two reasons. First, rotation effect on the luminosity-weighted velocity dispersion may not be significant as the integrated velocity dispersions are dominated by the inner part, where the rotation velocity is relatively small. In the case of the rotation-included velocity dispersion, the luminosity weight of the inner part is more dominant since velocity dispersions are integrated in quadrature (see Equation (1) in McConnell & Ma 2013). Second, since our sample is mainly composed of early-type galaxies, rotation effect is relatively weak compared to late-type galaxies. For late-type galaxies with a low σ_*, rotation effect can be significant, hence, it would be essential to correct for, in order to properly derive the $M_{\rm BH}$–σ_* relation.

For massive BHs, the sphere of influence of BH can be large enough to change the effective σ_* measurements since the velocity dispersion at the center increases due to the presence of a BH. Thus, by excluding the sphere of influence of BH in calculating the luminosity-weighted σ_*, the effective velocity dispersions will be decreased. Since these corrections can be done only for massive galaxies with a resolved sphere of influence, the slope of the $M_{\rm BH}$–σ_* relation will increase due to the preferential decrease of σ_* at high mass end. For example, by excluding the sphere of influence of BH in deriving the effective σ_* within R_e for 12 most massive galaxies, McConnell & Ma (2013) showed that the slope of the $M_{\rm BH}$–σ_* relation increased from 5.48 ± 0.30 to 5.64 ± 0.32. We performed a similar analysis using our data although only two galaxies, NGC 4486 and NGC 4649, are among those 12 galaxies with a resolved sphere of influence. By excluding the sphere of influence of BH, the luminosity-weighted σ_* decreases from 346 ± 12 to 327 ± 11 for NGC 4486, and from 346 ± 12 to 327 ± 11 for NGC 4649.

Based on these two updated σ_*, the slope of the $M_{\rm BH}$–σ_* relation slightly increases from 3.78 ± 0.43 to 3.79 ± 0.45; however, two slopes are consistent within the uncertainties. Using only two galaxies, it is not clear whether excluding or including the sphere of influence in determining the effective σ_* improves the $M_{\rm BH}$–σ_* relation.

Compared to the $M_{\rm BH}$–σ_* relation recently presented by McConnell & Ma (2013), we find a significantly shallower slope. They report a slope of 5.64 ± 0.32, using a much larger galaxy sample, which includes in particular more galaxies at higher and lower masses. We will investigate the implications of our results on the $M_{\rm BH}$–σ_* relation in detail in a companion paper (J.-H. Woo et al. 2013, in preparation).

5. SUMMARY

We observed a sample of 31 nearby galaxies with TripleSpec, a near-IR long-slit spectrograph at the Palomar 5 m telescope in order to homogeneously measure velocity dispersions from the H-band stellar lines. The galaxies in the sample cover a wide range in σ_* (67 km s^{-1} $< \sigma_* <$ 385 km s^{-1}) and their dynamical central BH masses are also available. To account for template mismatch, we used 11 giant stars with spectral type ranging from K0 to M5 as velocity templates, and found that M giants generate the most reliable fits and velocity dispersion measurements.

By measuring velocity and velocity dispersion as a function of radius along the major axis of each galaxy, we determined the rotation curve and velocity dispersion profile. Using these spatially resolved velocity dispersion measurements, we calculated the luminosity-weighted stellar velocity dispersions within the $R_{\rm e}$ of each galaxy. For 25 out of 31 galaxies in the sample, we found a clear rotation component, indicating that stellar velocity dispersions can be significantly overestimated due to the rotational broadening if a large single aperture is used to extract spectra. Compared to rotation-corrected velocity dispersions, velocity dispersions measured from single-aperture spectra showed systematically larger values by up to $\sim$20%.

We compared velocity dispersions measured from H-band stellar lines with those measured from optical lines and found no systematic difference, suggesting that optical and H-band stellar lines represent the same kinematics and that dust effect is negligible for early-type galaxies. Our results confirm that optical and near-IR stellar lines can be interchangeably used to measure stellar kinematics and near-IR σ_* measured for AGN host galaxies can be directly compared to optical σ_* of quiescent galaxies.

Using the rotation-corrected σ_* measurements based on the spatially resolved H-band spectra of 31 nearby galaxies, we derived the $M_{\rm BH}$–σ_* relation to investigate rotation effect. The slope of the $M_{\rm BH}$–σ_* relation is slightly shallower than that based on the rotation-included optical or near-IR σ_* measurements. Although rotation effect is not dramatically strong for early-type galaxies, it is potentially important to correct for, particularly for low-mass, late-type galaxies with a strong rotation component, in order to properly determine the $M_{\rm BH}$–σ_* relation and its intrinsic scatter. A future study based on spatially resolved spectra for late-type galaxies is required to fully quantify rotation effect on the $M_{\rm BH}$–σ_* relation.

We thank the anonymous referee for constructive suggestions, which improved the manuscript. This work was supported by the National Research Foundation of Korea (NRF) grant funded by the Korea government (MEST) (No. 2012-006087). J.H.W acknowledges the support by the Korea Astronomy and Space Science Institute (KASI) grant funded by the Korea government (MEST).

REFERENCES

Barth, A. J., Sarzi, M., Rix, H.-W., et al. 2001, ApJ, 555, 685
Bender, R., Saglia, R. P., & Gerhard, O. E. 1994, MNRAS, 269, 785
Bennert, V. N., Auger, M. W., Treu, T., Woo, J.-H., & Malkan, M. A. 2011a, ApJ, 726, 59
Bennert, V. N., Auger, M. W., Treu, T., Woo, J.-H., & Malkan, M. A. 2011b, ApJ, 742, 107
Bennert, V. N., Treu, T., Woo, J.-H., et al. 2010, ApJ, 708, 1507
Bower, G. A., Green, R. F., Bender, R., et al. 2001, ApJ, 550, 75
Bower, G. A., Green, R. F., Danks, A., et al. 1998, ApJL, 492, L111
Cretton, N., & van den Bosch, F. C. 1999, ApJ, 514, 704
Dasyra, K. M., Tacconi, L. J., Davies, R. I., et al. 2007, ApJ, 657, 102
Devereux, N., Ford, H., Tsvetanov, Z., & Jacoby, G. 2003, AJ, 125, 1226
Dressler, A. 1984, ApJ, 286, 97
Emsellem, E., Dejonghe, H., & Bacon, R. 1999, MNRAS, 303, 495
Ferrarese, L., & Ford, H. C. 1999, ApJ, 515, 583
Ferrarese, L., & Ford, H. 2005, SSRv, 116, 523
Ferrarese, L., Ford, H., & Jaffe, W. 1996, ApJ, 470, 444
Ferrarese, L., & Merritt, D. 2000, ApJL, 539, L9
Gebhardt, K., Adams, J., Richstone, D., et al. 2011, ApJ, 729, 119
Gebhardt, K., Bender, R., Bower, G., et al. 2000a, ApJL, 539, L13
Gebhardt, K., Richstone, D., Kormendy, J., et al. 2000b, AJ, 119, 1157
Gebhardt, K., Richstone, D., Tremaine, S., et al. 2003, ApJ, 583, 92
Graham, A. W. 2008, ApJ, 680, 143
Graham, A. W., Onken, C. A., Athanassoula, E., & Combes, F. 2011, MNRAS, 412, 2211
Gültekin, K., Richstone, D. O., Gebhardt, K., et al. 2009a, ApJ, 698, 198
Gültekin, K., Richstone, D. O., Gebhardt, K., et al. 2009b, ApJ, 695, 1577
Harris, C. E., Bennert, V. N., Auger, M. W., et al. 2012, ApJS, 201, 29
Herrnstein, J. R., Moran, J. M., Greenhill, L. J., & Trotter, A. S. 2005, ApJ, 629, 719
Kent, S. M. 1990, AJ, 100, 377
Kormendy, J., Bender, R., Evans, A., & Richstone, D. 1998, AJ, 115, 1823
Kormendy, J., & Gebhardt, K. 2001, in AIP Conf. Ser. 586, 20th Texas Symposium on Relativistic Astrophysics, ed. J. C. Wheeler & H. Martel (Melville, NY: AIP), 363
Lodato, G., & Bertin, G. 2003, A&A, 398, 517
Marconi, A., & Hunt, L. K. 2003, ApJL, 589, L21
McConnell, N. J., & Ma, C.-P. 2013, ApJ, 764, 184
McConnell, N. J., Ma, C.-P., Gebhardt, K., et al. 2011, Natur, 480, 215
McConnell, N. J., Ma, C.-P., Murphy, J. D., et al. 2012, ApJ, 756, 179
Nelson, C. H., & Whittle, M. 1995, ApJS, 99, 67
Onken, C. A., Ferrarese, L., Merritt, D., et al. 2004, ApJ, 615, 645
Park, D., Kelly, B. C., Woo, J.-H., & Treu, T. 2012, ApJS, 203, 6
Pinkney, J., Gebhardt, K., Bender, R., et al. 2003, ApJ, 596, 903
Rothberg, B., & Fischer, J. 2010, ApJ, 712, 318
Sani, E., Marconi, A., Hunt, L. K., & Risaliti, G. 2011, MNRAS, 413, 1479
Sarzi, M., Rix, H.-W., Shields, J. C., et al. 2001, ApJ, 550, 65
Schulze, A., & Gebhardt, K. 2011, ApJ, 729, 21
Shen, J., & Gebhardt, K. 2010, ApJ, 711, 484
Silge, J. D., & Gebhardt, K. 2003, AJ, 125, 2809
Smith, E. P., Heckman, T. M., & Illingworth, G. D. 1990, ApJ, 356, 399
Tremaine, S., Gebhardt, K., Bender, R., et al. 2002, ApJ, 574, 740
van den Bosch, F. C., & van der Marel, R. P. 1995, MNRAS, 274, 884
van den Bosch, R. C. E., & de Zeeuw, P. T. 2010, MNRAS, 401, 1770
Vanderbeke, J., Baes, M., Romanowsky, A. J., & Schmidtobreick, L. 2011, MNRAS, 412, 2017
van der Marel, R. P. 1994, MNRAS, 270, 271
van der Marel, R. P., Binney, J., & Davies, R. L. 1990, MNRAS, 245, 582
van der Marel, R. P., Cretton, N., de Zeeuw, P. T., & Rix, H.-W. 1998, ApJ, 493, 613
van der Marel, R. P., & van den Bosch, F. C. 1998, AJ, 116, 2220
Verolme, E. K., Cappellari, M., Copin, Y., et al. 2002, MNRAS, 335, 517
Walsh, J. L., Barth, A. J., & Sarzi, M. 2010, ApJ, 721, 762
Watson, L. C., Martini, P., Dasyra, K. M., et al. 2008, ApJL, 682, L21
Woo, J.-H., Treu, T., Barth, A. J., et al. 2010, ApJ, 716, 269
Woo, J.-H., Treu, T., Malkan, M. A., & Blandford, R. D. 2006, ApJ, 645, 900
Woo, J.-H., Treu, T., Malkan, M. A., & Blandford, R. D. 2008, ApJ, 681, 925
Woo, J.-H., Urry, C. M., Lira, P., van der Marel, R. P., & Maza, J. 2004, ApJ, 617, 903
Woo, J.-H., Urry, C. M., van der Marel, R. P., Lira, P., & Maza, J. 2005, ApJ, 631, 762